Mechanical Load Fault Detection in Induction Motors by Stator Current Time-Frequency Analysis

Martin Blödt, *Student Member, IEEE*, Marie Chabert, Jérémi Regnier, and Jean Faucher, *Member, IEEE*

***Abstract*—This paper examines the detection of mechanical faults in induction motors by an original use of stator current time-frequency analysis. Mechanical faults lead generally to periodic load torque oscillations. The influence of the torque oscillations on the induction motor stator current is studied using an analytical approach. The mechanical fault results in a sinusoidal phase modulation of the stator current, which is equivalent to a time-varying frequency. Based on these assumptions, several signal processing methods suitable for stator current signature analysis are discussed: classical spectral analysis, instantaneous frequency estimation, and the Wigner distribution. Experimental and simulation results validate the theoretical approach in steady-state operating conditions.**

***Index Terms*—Induction motor fault diagnosis, load unbalance, mechanical fault, time-frequency analysis, torque oscillations.**

I. Introduction

INDUCTION motors are used in a wide variety of industrial applications. In order to increase the productivity, reliability, and safety of an installation containing induction motors, permanent and automatic motor condition monitoring is required.

Generally, the motor condition can be supervised by measuring quantities such as noise, vibration, and temperature. The implementation of such measuring systems is expensive and proves only to be economical in the case of large motors or critical applications. A solution to this problem can be the use of quantities that are already measured in a drive system, e.g., the machine's stator current, which is often required for control or protection purposes.

This paper investigates the detection of torque oscillations caused by mechanical faults in induction machines using stator current time-frequency analysis. In a general way, a fault in the load part of the drive is seen from the induction machine by a variation of the load torque that is no longer constant. Examples for such faults causing torque oscillations include:

1) general fault in the load part of the drive system, e.g., mechanical imbalance, shaft misalignment;
2) gearbox faults, e.g., broken tooth;
3) bearing faults.

Torque oscillations already exist in a healthy motor due to space and time harmonics of the airgap field. However, the fault-induced torque oscillations are present at particular frequencies, often related to the mechanical motor speed.

Thomson mentioned in [1] that mechanical problems in the load may cause speed oscillations that modulate the motor input current and lead to additional frequencies in the current spectrum. Schoen and Habetler have shown in [2] that load torque oscillations appearing at multiples of the rotational speed lead to peaks in the stator current spectrum at frequencies

$$f_{\text{load}} = f_s \pm n f_r \tag{1}$$

where f_s is the stator supply frequency, f_r is the rotational frequency, and $n = 1, 2, 3, \ldots$ These sidebands are used in [3] for mechanical fault detection. This paper provides a more accurate analysis of the type of modulation appearing on the stator current in case of a load torque oscillation.

In Section II, the influence of load torque oscillations on the stator current is studied using a magnetomotive force (MMF) wave approach. It is shown that this type of fault leads to a phase modulation of a stator current component. Different methods for detection such as classical spectral analysis and time-frequency methods are presented in Section III. In Section IV, some simulation results illustrate the theoretical development. Experimental results are discussed more extensively in Section V where the different fault detection techniques are demonstrated with load torque oscillations and a load unbalance.

II. Influence of Torque Oscillations on Stator Current

The method used to study the influence of the periodic load torque variation on the stator current is based on the MMF and permeance wave approach [4], [5]. This approach is traditionally used for the calculation of the magnetic airgap field with respect to rotor and stator slotting or static and dynamic eccentricity [6], [7].

First, the rotor and stator MMFs are calculated, which are directly related to the current flowing in the windings. The

Paper IPCSD-06-040, presented at the 2005 IEEE International Electric Machines and Drives Conference, San Antonio, TX, May 15–18, and approved for publication in the IEEE Transactions on Industry Applications by the Electric Machines Committee. Manuscript submitted for review July 30, 2005 and released for publication June 24, 2006.

M. Blödt, J. Regnier, and J. Faucher are with the Laboratoire d'Electrotechnique et d'Electronique Industrielle (LEEI), 31071 Toulouse Cedex 7, France (e-mail: Martin.Blodt@leei.enseeiht.fr; regnier@leei.enseeiht.fr; Jean.Faucher@leei.enseeiht.fr).

M. Chabert is with the Laboratory Télécommunications Spatiales et Aéronautiques (TéSA) and the Institut de Recherche en Informatique de Toulouse (IRIT), 31071 Toulouse Cedex 7, France (e-mail: Marie.Chabert@enseeiht.fr).

Digital Object Identifier 10.1109/TIA.2006.882631

second important quantity is the airgap permeance Λ, which is directly proportional to the inverse of the airgap length g. The magnetic field in the airgap can then be determined by multiplying the permeance by the sum of rotor and stator MMFs. The equivalent magnetic flux in one phase is obtained by integration of the magnetic field in each turn of the phase winding. The induced phase voltage, related to the current by the stator voltage equation, is then deduced from the magnetic flux. This method has been used by the authors in [8] to identify the consequence of bearing fault related load torque oscillations on the stator current.

A. Effect on Rotor MMF

Under a mechanical fault, the load torque as a function of time is modeled by a constant component Γ_{const} and an additional component varying at the characteristic frequency f_c (which can be for example the rotational frequency f_r). The first term of the variable component Fourier series is a cosine with frequency f_c. For the sake of clarity, higher order terms are neglected in the following, and only the fundamental term is considered. The load torque can therefore be described by

$$\Gamma_{\text{load}}(t) = \Gamma_{\text{const}} + \Gamma_c \cos(\omega_c t) \tag{2}$$

where Γ_c is the amplitude of the load torque oscillation and $\omega_c = 2\pi f_c$.

The machine mechanical equation relates the torque oscillation to the motor speed ω_r as follows:

$$\begin{aligned}\sum \Gamma(t) &= \Gamma_{\text{motor}}(t) - \Gamma_{\text{load}}(t) \\ &= J\frac{d\omega_r}{dt} \Leftrightarrow \omega_r(t) \\ &= \frac{1}{J}\int_t \left(\Gamma_{\text{motor}}(\tau) - \Gamma_{\text{load}}(\tau)\right) d\tau \end{aligned} \tag{3}$$

where Γ_{motor} is the electromagnetic torque produced by the machine and J is the total inertia of the machine and the load.

In steady state, the motor torque Γ_{motor} is equal to the constant part Γ_{const} of the load torque. The mechanical speed is then expressed as

$$\begin{aligned}\omega_r(t) &= -\frac{1}{J}\int_{t_0}^{t} \Gamma_c \cos(\omega_c \tau) d\tau + C \\ &= -\frac{\Gamma_c}{J\omega_c}\sin(\omega_c t) + \omega_{r0}. \end{aligned} \tag{4}$$

The mechanical speed consists therefore of a constant component ω_{r0} and a sinusoidally varying one.

Finally, the mechanical speed integration provides the mechanical rotor position θ_r

$$\theta_r(t) = \int_{t_0}^{t} \omega_r(\tau) d\tau = \frac{\Gamma_c}{J\omega_c^2}\cos(\omega_c t) + \omega_{r0} t. \tag{5}$$

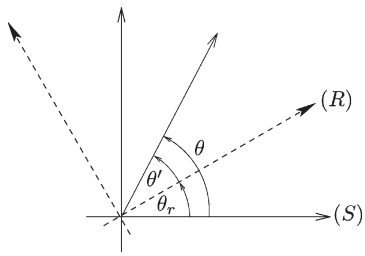

Fig. 1. Stator (*S*) and rotor (*R*) reference frame.

The integration constant has been assumed to be zero. In contrast to the healthy machine where $\theta_r(t) = \omega_{r0} t$, oscillations at the characteristic frequency are present on the mechanical rotor position.

The oscillations of the mechanical rotor position θ_r act on the rotor MMF. In a normal state, the rotor MMF in the rotor reference frame (R) is a wave with p pole pairs and a frequency sf_s, given by

$$F_r^{(R)}(\theta', t) = F_r \cos(p\theta' - s\omega_s t) \tag{6}$$

where θ' is the mechanical angle in the rotor reference frame (R) and s is the motor slip. Higher order space and time harmonics are neglected.

Fig. 1 displays the transformation between the rotor and stator reference frame, defined by $\theta = \theta' + \theta_r$. Using (5), this leads to

$$\theta' = \theta - \omega_{r0} t - \frac{\Gamma_c}{J\omega_c^2}\cos(\omega_c t). \tag{7}$$

Thus, the rotor MMF given in (6) can be transformed to the stationary stator reference frame using (7) and the relation $\omega_{r0} = \omega_s(1-s)/p$

$$F_r(\theta, t) = F_r \cos\left(p\theta - \omega_s t - \beta\cos(\omega_c t)\right) \tag{8}$$

with

$$\beta = p\frac{\Gamma_c}{J\omega_c^2}. \tag{9}$$

Equation (8) clearly shows that the torque oscillations at frequency f_c lead to a phase modulation of the rotor MMF in the stator reference frame. This phase modulation is characterized by the introduction of the term $\beta\cos(\omega_c t)$ in the phase of the MMF wave. The parameter β is generally called the modulation index. For physically reasonable values J, Γ_c, and ω_c, the approximation $\beta \ll 1$ holds in most cases.

The fault has no direct effect on the stator MMF, and so, it is considered to have the following form:

$$F_s(\theta, t) = F_s \cos(p\theta - \omega_s t - \varphi_s) \tag{10}$$

where φ_s is the initial phase difference between rotor and stator MMFs. As in the case of the rotor MMF, only the fundamental space and time harmonic is taken into account; higher order space and time harmonics are neglected.

B. Effect on Flux Density and Stator Current

The airgap flux density $B(\theta,t)$ is the product of total MMF and airgap permeance Λ. The airgap permeance is supposed constant because slotting effects and eccentricity are not taken into account for the sake of clarity and simplicity

$$\begin{aligned} B(\theta,t) &= [F_s(\theta,t) + F_r(\theta,t)]\,\Lambda \\ &= B_s \cos(p\theta - \omega_s t - \varphi_s) \\ &\quad + B_r \cos(p\theta - \omega_s t - \beta\cos(\omega_c t)). \end{aligned} \tag{11}$$

The phase modulation of the flux density $B(\theta,t)$ exists for the flux $\Phi(t)$ itself, as $\Phi(t)$ is obtained by a simple integration of $B(\theta,t)$ with respect to the winding structure. The winding structure has only an influence on the amplitudes of the flux harmonic components, not on their frequencies. Therefore, $\Phi(t)$ in an arbitrary phase can be expressed in a general form

$$\Phi(t) = \Phi_s \cos(\omega_s t + \varphi_s) + \Phi_r \cos(\omega_s t + \beta\cos(\omega_c t)). \tag{12}$$

The relation between the flux and the stator current in a considered phase is given by the stator voltage equation

$$V(t) = R_s I(t) + \frac{d\Phi(t)}{dt}. \tag{13}$$

With $V(t)$ imposed by the voltage source, the resulting stator current will be in a linear relation to the time derivative of the phase flux $\Phi(t)$ and will have an equivalent frequency content. Differentiating (12) leads to

$$\begin{aligned} \frac{d}{dt}\Phi(t) &= -\omega_s\Phi_s \sin(\omega_s t + \varphi_s) - \omega_s\Phi_r \sin(\omega_s t + \beta\cos(\omega_c t)) \\ &\quad + \omega_c\beta\Phi_r \sin(\omega_s t + \beta\cos(\omega_c t))\sin(\omega_c t). \end{aligned} \tag{14}$$

The amplitude of the last term is smaller than the amplitude of the other terms because $\beta \ll 1$. Thus, the last term in (14) will be neglected in the following.

As a consequence, the stator current in an arbitrary phase can be expressed in a general form

$$\begin{aligned} I(t) &= i_{\mathrm{st}}(t) + i_{\mathrm{rt}}(t) \\ &= I_{\mathrm{st}} \sin(\omega_s t + \varphi_s) + I_{\mathrm{rt}} \sin(\omega_s t + \beta\cos(\omega_c t)). \end{aligned} \tag{15}$$

Therefore, the stator current $I(t)$ can be considered as the sum of two components. The term $i_{\mathrm{st}}(t)$ results from the stator MMF, and it is not modulated. The term $i_{\mathrm{rt}}(t)$, which is a direct consequence of the rotor MMF, shows the phase modulation due to the considered load torque oscillations. The healthy case is obtained for $\beta = 0$.

In this paper, the time harmonics of the rotor MMF and the non-uniform airgap permeance have not been considered. However, the harmonics of supply frequency f_{s} and the rotor slot harmonics will theoretically show the same phase modulation as the fundamental component.

III. Signal Processing Methods

The previous section has shown that the load torque oscillations cause a phase modulation on one stator current component according to (15). It should be noticed that the signal is not stationary in the faulty case due to the time-varying phase. In order to detect the phase modulation, several signal processing methods can be used. In the following paragraphs, three methods will be presented, and their performances will be discussed.

In order to simplify calculations, all signals will be considered in their complex form, the so-called analytical signal [9], [10]. The analytical signal $z(t)$ is related to the real signal $x(t)$ via the Hilbert Transform $H\{.\}$

$$z(t) = x(t) + jH\{x(t)\}. \tag{16}$$

The analytical signal contains the same information as the real signal, but its Fourier transform (FT) is zero at negative frequencies.

A. Power Spectral Density (PSD)

1) Definition: The classical method for signal analysis in the frequency domain is the estimation of the PSD based on the discrete FT of the signal x. The PSD indicates the distribution of signal energy with respect to frequency. The common estimation method for the PSD is the periodogram $P_{xx}(f)$ [11], which is defined as the square of the signal's N-point FT divided by N

$$P_{xx}(f) = \frac{1}{N}\left|\sum_{n=0}^{N-1} x(n) e^{-\mathrm{j}2\pi f n}\right|^2. \tag{17}$$

2) Application: The PSD represents the basic signal analysis tool for stationary signals. However, in case of the considered fault, the stator current signal is no longer strictly stationary, because the frequency of one signal component is varying sinusoidally in time.

In the case of a constant supply frequency f_s, the PSD can nevertheless be used to analyze the signal, considering the phase-modulated signal component given in a complex form by

$$i_{\mathrm{rt}}(t) = I_{\mathrm{rt}} \exp j(\omega_s t + \beta\cos(\omega_c t)). \tag{18}$$

Its FT is well known from communication theory [12], and it can be expressed as follows:

$$I_{\mathrm{rt}}(f) = I_{\mathrm{rt}} \sum_{n=-\infty}^{+\infty} j^n J_n(\beta)\delta(f - (f_s + nf_c)) \tag{19}$$

where J_n denotes the nth-order Bessel function of the first kind and $\delta(f)$ is the Dirac delta function. For small modulation indexes β, the Bessel functions of order $n \geq 2$ are very small and may be neglected (narrowband approximation).

Using this approximation, the absolute value of the FT $|I(f)|$ of the stator current (15) in the faulty case can be written as

$$|I(f)| = (I_{\mathrm{st}} + I_{\mathrm{rt}} J_0(\beta))\,\delta(f - f_s) + I_{\mathrm{rt}} J_1(\beta)\delta\left(f - (f_{\mathrm{s}} \pm f_c)\right). \quad (20)$$

It becomes clear through this expression that the fault leads to sideband components of the fundamental at $f_s \pm f_c$.

However, the major disadvantage of the PSD is that there exist other phenomena such as different forms of eccentricity [7] or bearing faults [8] that may cause spectral components at the same frequencies. Other types of modulation such as amplitude modulation have a similar effect on the PSD. Moreover, most stator current spectra will already contain these frequencies in practice due to an inherent level of eccentricity.

B. Instantaneous Frequency (IF)

1) Definition: For a complex monocomponent signal $z(t) = a(t)e^{j\varphi(t)}$, the IF $f_i(t)$ is defined by [9]

$$f_i(t) = \frac{1}{2\pi}\frac{d}{dt}\varphi(t) \quad (21)$$

where $\varphi(t)$ is the instantaneous phase and $a(t)$ is the instantaneous amplitude of the analytical signal $z(t)$.

2) Application: The IF of a monocomponent phase-modulated signal can be calculated using the definition (21). For the phase-modulated stator current component related to the rotor MMF [see (18)], it can be expressed as

$$f_{i,i_{\mathrm{rt}}}(t) = f_s - f_c\beta\sin(\omega_c t). \quad (22)$$

The fault therefore has a direct effect on the IF of the stator current component $i_{\mathrm{rt}}(t)$. In the healthy case, its IF is constant; in the faulty case, a time-varying component with frequency f_c appears.

If the complex multicomponent signal according to (15) is considered, the calculation of its IF leads to the following expression:

$$f_{i,I}(t) = f_s - f_c\beta\sin(\omega_c t)\frac{1}{1 + a(t)} \quad (23)$$

with

$$a(t) = \frac{I_{\mathrm{st}}^2 + I_{\mathrm{st}} I_{\mathrm{rt}}\cos\left(\beta\cos(\omega_c t) - \varphi_s\right)}{I_{\mathrm{rt}}^2 + I_{\mathrm{st}} I_{\mathrm{rt}}\cos\left(\beta\cos(\omega_c t) - \varphi_s\right)}. \quad (24)$$

Using reasonable approximations, it can be shown that $1/(1 + a(t))$ is composed of a constant component with only small oscillations. Hence, the IF of (15) may be approximated by

$$f_{i,I}(t) \approx f_s - C f_c\beta\sin(\omega_c t) \quad (25)$$

where C is a constant, $C < 1$. Numerical evaluations confirm this approximation. It can therefore be concluded, that the multicomponent signal IF corresponding to the stator current also shows fault-related oscillations at f_c, which may be used for detection.

C. Wigner Distribution (WD)

1) Definition: The WD can be interpreted as a distribution of the signal energy in function of time and frequency. It is defined as follows [10]:

$$W_x(t,f) = \int_{-\infty}^{+\infty} x\left(t + \frac{\tau}{2}\right) x^*\left(t - \frac{\tau}{2}\right) e^{-j2\pi f\tau} d\tau. \quad (26)$$

This formula can be seen as the FT of a kernel $K_x(\tau, t)$ with respect to the delay variable τ. The kernel is similar to an autocorrelation function.

An interesting property of the WD is its perfect concentration on the IF in the case of a linear frequency modulation. However, other types of modulations (e.g., in our case, sinusoidal phase modulations) produce so-called inner interference terms in the distribution [13]. Note that the interferences may, however, be used for detection purposes as it will be shown in the following.

Another important drawback of the distribution is its nonlinearity due to the quadratic nature. When the sum of two signals is considered, so-called outer interference terms appear in the distribution at time instants or frequencies where there should not be any signal energy [13].

In practice, the pseudo WD (PWD), which is a smoothed version of the WD, is often used. PWD is defined as

$$\mathrm{PW}_x(t,f) = \int_{-\infty}^{+\infty} p(\tau) x\left(t + \frac{\tau}{2}\right) x^*\left(t - \frac{\tau}{2}\right) e^{-j2\pi f\tau} d\tau \quad (27)$$

where $p(\tau)$ is the smoothing window which reduces the amplitudes of the interference terms.

2) Application: In order to obtain the WD of the stator current according to (15), the WD of a pure phase-modulated signal $i_{\mathrm{rt}}(t)$ [see (18)] will first be calculated.

The WD kernel of a phase-modulated signal can be written as

$$K_{i_{\mathrm{rt}}}(t,\tau) = i_{\mathrm{rt}}\left(t + \frac{\tau}{2}\right) i_{\mathrm{rt}}^*\left(t - \frac{\tau}{2}\right) = I_{\mathrm{rt}}^2 \exp j\left\{\omega_s\tau - 2\beta\sin(\omega_c t)\sin\left(\frac{\omega_c}{2}\tau\right)\right\}. \quad (28)$$

The WD is obtained as the FT of the kernel with respect to the delay τ

$$W_{i_{\mathrm{rt}}}(t,f) = \mathrm{FT}_\tau\left\{K_{i_{\mathrm{rt}}}(t,\tau)\right\} = I_{\mathrm{rt}}^2 \mathrm{FT}_\tau\left\{\exp j(\omega_s\tau)\right\} * \mathrm{FT}_\tau\left\{\exp j\left[-2\beta\sin(\omega_c t)\sin\left(\frac{\omega_c}{2}\tau\right)\right]\right\} \quad (29)$$

where $*$ denotes the convolution. The FT of the second term may be calculated in analogy to the FT of a pure phase-modulated signal [see (19)] using the Jacobi–Anger expansion [14] given by

$$e^{j\gamma\sin\theta} = \sum_{n=-\infty}^{+\infty} J_n(\gamma) e^{jn\theta}. \quad (30)$$

The second term in (29) can therefore be developed into a Fourier series which allows a simple calculation of its FT

$$\begin{aligned} W_{i_{\rm rt}}(t,f) &= I_{\rm rt}^2\delta(f-f_s) \\ &\quad * \mathrm{FT}_\tau\left\{\sum_{n=-\infty}^{+\infty} J_n\left(-2\beta\sin(\omega_c t)\right)e^{jn\frac{\omega_c}{2}\tau}\right\} \\ &= I_{\rm rt}^2\sum_{n=-\infty}^{+\infty} J_n\left(-2\beta\sin(\omega_c t)\right)\delta\left(f-f_s-n\frac{f_c}{2}\right). \end{aligned} \tag{31}$$

For small modulation indexes β, the narrowband approximation leads to

$$\begin{aligned} W_{i_{\rm rt}}(t,f) &\approx I_{\rm rt}^2 J_0(\gamma)\delta(f-f_s) \\ &\quad + I_{\rm rt}^2 J_1(\gamma)\delta\left(f-f_{\rm s}-\frac{f_c}{2}\right) \\ &\quad - I_{\rm rt}^2 J_1(\gamma)\delta\left(f-f_s+\frac{f_c}{2}\right) \end{aligned} \tag{32}$$

with $\gamma = -2\beta\sin(\omega_c t)$.

The WD of the considered pure phase-modulated signal is therefore a central frequency at f_s with sidebands at $f_s \pm f_c/2$. All the components have time-varying amplitudes at frequency f_c, as γ is a function of time. It is important to notice that the lower sideband has the opposed sign to the upper sideband.

As the stator current signal is considered as the sum of two components, a phase-modulated signal and a pure frequency [see (15)], its WD must be calculated according to the following expression for the sum of two signals $x+y$ [10]:

$$W_{x+y}(t,f) = W_x(t,f) + W_y(t,f) + 2\mathrm{Re}\left\{W_{xy}(t,f)\right\} \tag{33}$$

with

$$W_{xy}(t,f) = \int_{-\infty}^{+\infty} x\left(t+\frac{\tau}{2}\right)y^*\left(t-\frac{\tau}{2}\right)e^{-j2\pi f\tau}d\tau. \tag{34}$$

The WD of the pure frequency $i_{\rm st}(t) = I_{\rm st}\sin(\omega_s t+\varphi_s)$ [first term of (15)] is given by $I_{\rm st}^2\delta(f-f_s)$. A detailed calculation of the cross terms $W_{i_{\rm st}i_{\rm rt}}$ shows that they are of small amplitude and that they do not introduce new frequency components. Thus, the cross terms may be neglected in this case, and the following approximate expression is obtained for the WD of (15):

$$\begin{aligned} W_{i_{\rm st}+i_{\rm rt}}(t,f) &\approx \left(I_{\rm rt}^2 J_0(\gamma) + I_{\rm st}^2\right)\delta(f-f_s) \\ &\quad + I_{\rm rt}^2 J_1(\gamma)\delta\left(f-f_{\rm s}-\frac{f_c}{2}\right) \\ &\quad - I_{\rm rt}^2 J_1(\gamma)\delta\left(f-f_s+\frac{f_c}{2}\right). \end{aligned} \tag{35}$$

In contrast to the pure phase-modulated signal, the constant component $I_{\rm st}$ is present at the fundamental frequency. In a logarithmic plot, this constant component will hide the oscillations of the fundamental due to its greater amplitude, and the frequency f_s will appear constant in time as can be seen in the experimental results.

D. Spectrogram

The spectrogram is a time-frequency distribution based on the FT of the product of a sliding window $h(t)$ with the signal. It is given by the following expression for a signal $x(t)$ [10]:

$$S_x(t,f) = \left|\int_{-\infty}^{+\infty} x(\tau)h^*(\tau-t)e^{-j2\pi f\tau}d\tau\right|^2. \tag{36}$$

In comparison to the WD, the spectrogram shows no interference terms outside the signal components time-frequency support in case of multicomponent signals or nonlinear frequency modulations. However, a great disadvantage is the reduced resolution power compared to the WD. The length of the sliding window $h^*(t)$ determines time and frequency resolution, i.e., a good frequency resolution needs a long observation window and therefore leads to a bad localization in time and vice versa [10]. Moreover, the window length has to be chosen based on a prior knowledge of the signal.

E. Summary

It has been shown that several signal processing methods can be used for the detection of load torque oscillations. Classical spectral analysis based on the PSD can give a first indication of a possible fault by an increase of sidebands at $f_s \pm f_r$. As other phenomena produce similar sidebands, it is not possible to identify the phase modulations without ambiguity. The IF can be used to detect phase modulations if the signal is monocomponent. A global time-frequency signal analysis is possible using the WD or PWD where a characteristic interference structure appears in presence of the phase modulations. The spectrogram is a time-frequency distribution with limited resolution, so that it is not suitable for a direct stator current analysis. However, it will be shown in the following that it can effectively be used in combination with the IF estimation.

IV. Simulation Results

Simulations have been carried out using two different machine models: first, a standard space phasor model in the stationary reference frame, and second, a more detailed machine model based on magnetically coupled electric circuits [15]. Both simulations show that the predicted interference structure is visible on the PWD of the current signals with load torque oscillations. As an example, the machine has been loaded with 15-N $\cdot$ m average torque (nominal torque is 35 N $\cdot$ m) and a torque oscillation with amplitude $\Gamma_c = 0.2$ N $\cdot$ m, and frequency $f_c = f_r \approx f_s/p$ has been turned on in the middle of the simulation. Then, the PWD of both current signals is calculated. Fig. 2 shows the result from the model based on magnetically coupled electric circuits, Fig. 3 from the space phasor simulation. The theoretically calculated interference

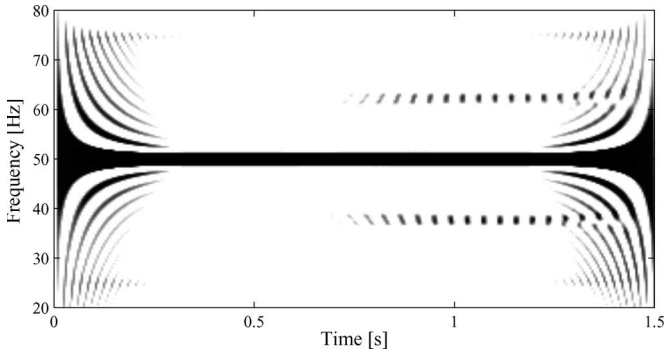

Fig. 2. PWD of simulated current signal with apparition of load torque oscillation (magnetically coupled electric circuits).

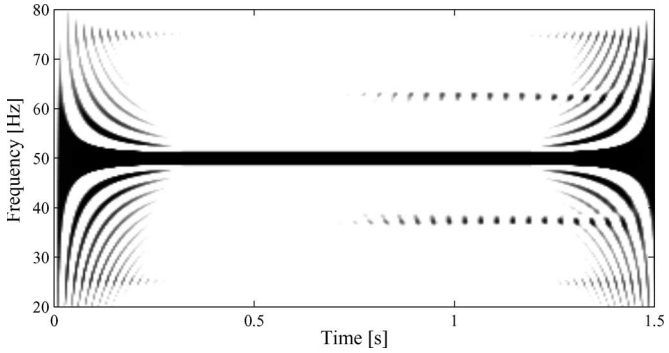

Fig. 3. PWD of simulated current signal with apparition of load torque oscillation (space phasor model).

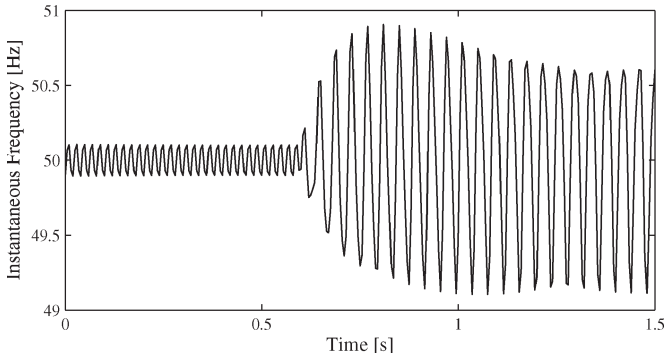

Fig. 4. IF of simulated current signal with apparition of load torque oscillation (magnetically coupled electric circuits).

structure at $f_s \pm f_c/2$ is clearly visible in both time-frequency distributions. Only slight differences in amplitude exist between the two simulations. Further simulations at higher and lower load levels always show the same effects on the PWD.

The calculation of the stator current IF for the previous signal leads to the result displayed in Fig. 4. Small oscillations are already present in the healthy current IF. The load torque oscillation starting at 0.6 s leads to significant IF oscillations.

As the simulations agree with the theory and the experimental results, only the last will be commented in details. As a conclusion, it can be stated that the simple machine model is well suited to correctly represent the effect of the load torque oscillation, and therefore, there is no need in this case for a time-intensive and detailed simulation.

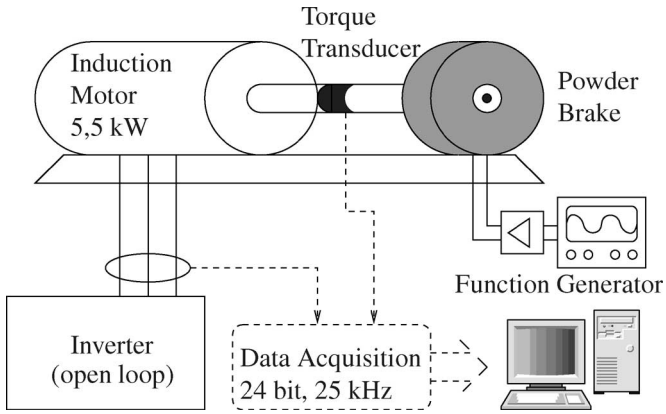

Fig. 5. Scheme of experimental setup.

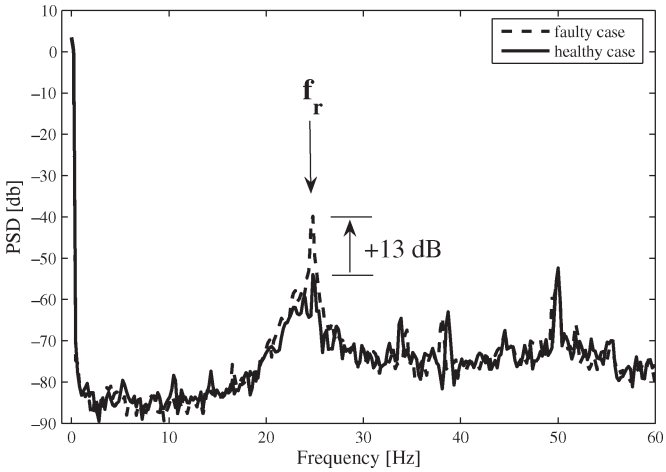

Fig. 6. PSD of the measured torque in healthy case and with small load torque oscillation.

V. Experimental Results

A. Experimental Setup

Tests have been conducted on a test rig with a 5.5-kW Leroy Somer induction machine (see Fig. 5). The motor has two pole pairs and a nominal torque of 35 N · m. The machine is supplied by a standard industrial inverter with a constant voltage-to-frequency ratio. The load is a magnetic powder brake supplied by a function generator coupled to a voltage-controlled oscillator. This allows the production of periodic load torque oscillations. The load torque is measured by a rotating torque transducer. The torque signal, current, and voltage measurements are acquired at a sampling rate of 25 kHz by a 24-bit data-acquisition board. The further signal processing is done using Matlab and the time-frequency toolbox [16].

B. Results at Small Load

The powder brake is used to produce an oscillating load torque at the rotational frequency which is slightly inferior to 25 Hz. The motor is loaded in the first tests with about 9-N · m average torque (recall that its nominal torque is about 35 N · m).

The measured load torque (see Fig. 6) shows an increase of its spectral component at 25 Hz of about 13 dB between the faulty and the healthy case, which confirms that the

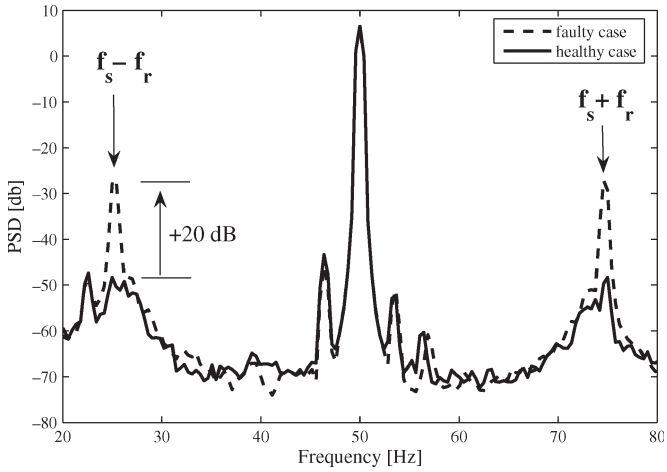

Fig. 7. PSD of measured stator current in healthy case and with small load torque oscillation.

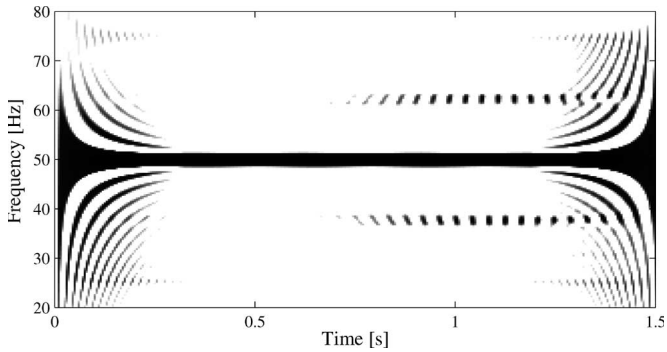

Fig. 8. PWD of measured current signal with apparition of load torque oscillation.

powder brake produces correctly the load torque oscillations. The amplitude of the torque oscillations is about 1% (−40 dB on the PSD) of the amplitude of the constant component which corresponds to 0.09 N · m.

The effect of the torque oscillation on the stator current can clearly be observed in Fig. 7 where the PSD of the stator current is shown for the healthy and the faulty case. Spectral components at $f_s \pm f_r$ can already be noticed in the healthy state due to phenomena like a natural level of eccentricity. In the faulty case with a small load torque oscillation, these components show a considerable increase of about 20 dB. The apparition of these sidebands corresponds to the theoretical prediction in (20).

In another test, the load torque oscillations of the same amplitude as before have been turned on in the middle of a data acquisition in order to study a sudden fault apparition. In this case, the classical spectral analysis is not an adequate tool any more, because the signal is a transient nonstationary signal. The stator current has therefore been analyzed using a time-frequency distribution, the PWD, which is a smoothed version of the WD [10]. The result is shown in Fig. 8. When the load torque oscillation appears, an interference structure becomes visible in the PWD. As the stator current is a multicomponent signal due to supply harmonics, the signal has been low-pass filtered at twice the fundamental frequency and downsampled before calculating the PWD.

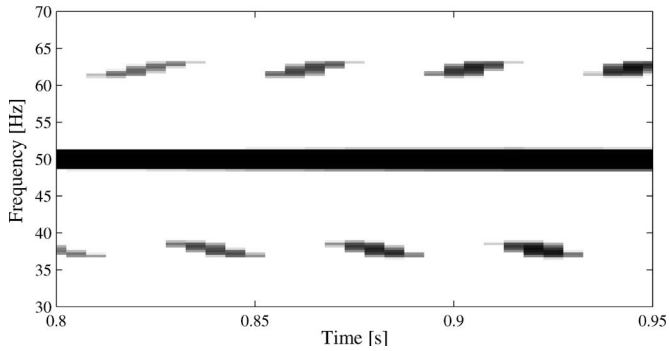

Fig. 9. Zoom on PWD of the measured current signal with load torque oscillation.

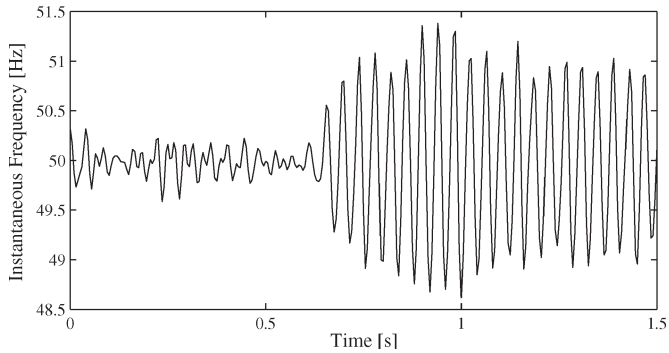

Fig. 10. Stator current IF with apparition of load torque oscillation.

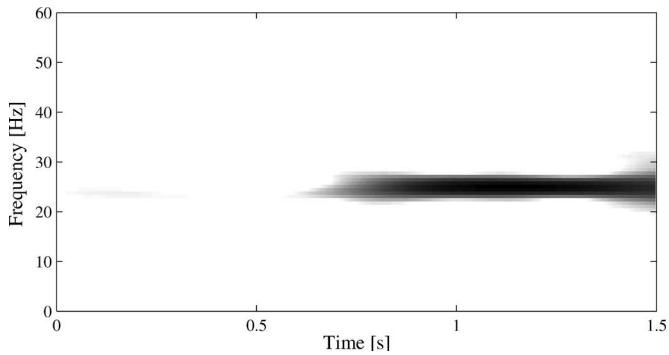

Fig. 11. Spectrogram of stator current IF with apparition of load torque oscillation.

A zoom on the interference structure (see Fig. 9) reveals that it corresponds to the theoretical WD calculated in the preceding section [see (32)]. The interference terms are sideband components at $f_s \pm f_c/2$ with opposed amplitudes for a given time instant. It is also visible that the sidebands are oscillating at 25 Hz as predicted in the theoretical development.

Another possibility to analyze the current signal is the estimation of its IF. If the signal is low-pass filtered at twice the fundamental frequency, it can be considered as a monocomponent signal, and its IF has a physical sense. The stator current IF estimation is shown at Fig. 10. In a healthy condition, the IF of the stator current fundamental is theoretically a constant signal at $f_s = 50$ Hz, but in reality, it shows small oscillations. When the fault appears at 0.6 s, the IF starts to oscillate at the

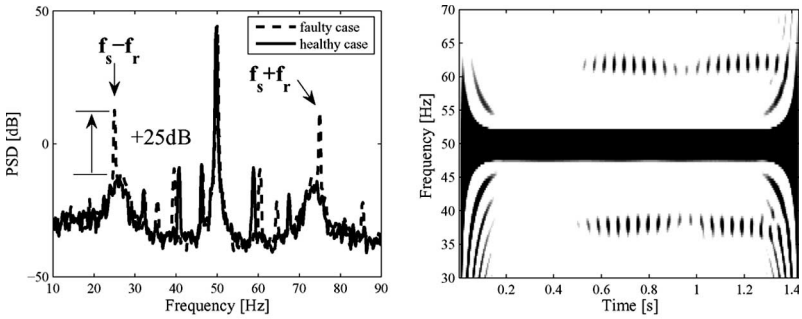

Fig. 12. PSD and PWD of measured current signal with apparition of load torque oscillation, higher load. (a) PSD. (b) PWD.

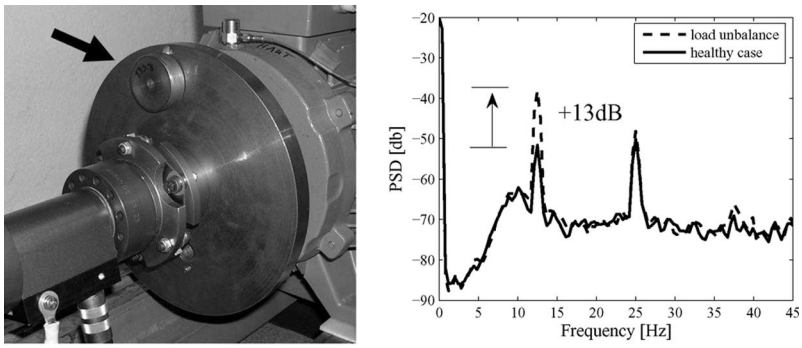

Fig. 13. Photograph of unbalanced load and PSD of measured torque with and without load unbalance. (a) Unbalanced load. (b) PSD of measured torque.

fault characteristic frequency f_c, which is in this case about 25 Hz. This result validates the theoretical considerations in the preceding sections.

An interesting alternative to the IF time-domain analysis can be a time-frequency representation of the IF. Fig. 11 shows the spectrogram of the stator current IF. It is clearly visible that at the instant of the fault, a spectral component appears at about 25 Hz. Before the calculation of the spectrogram, the average value of the IF has been subtracted in order to remove unnecessary information. Time-frequency analysis of the stator current IF can therefore provide a good fault indicator.

C. Results at Higher Load

In order to test the methods under heavier load, the average load torque has been increased to about 20 N · m. The measured load torque shows an increase of 12 dB at the characteristic frequency f_c compared to the healthy case. The amplitude of the measured torque oscillations is about 1/700 of the amplitude of the constant component, which corresponds to 0.03 N · m.

The PSD of the healthy and faulty current under load condition is shown in Fig. 12(a). The results are very similar to the preceding case with only a small load. The spectral lines at $f_s \pm f_r$ show a considerable increase in presence of the fault.

A time-frequency analysis of the stator current signal with an appearing load torque oscillation is shown in Fig. 12(b). The PWD shows the same fault-related interference structure as in the tests under small load. The application of the other methods used in the preceding section showed the same results.

D. Results With Load Unbalance

Until now, only torque oscillations produced by a powder brake were studied. In order to produce a realistic mechanical fault, a load unbalance is introduced. A small mass m is fixed on a disk mounted on the motor shaft [see Fig. 13(a)]. Different distances r from the center can be chosen. This load unbalance theoretically creates a sinusoidal load torque oscillation at rotational frequency f_r and with amplitude $\Gamma_c = mgr$, where g is the acceleration of gravity. Furthermore, an additional centrifugal force acts on the shaft, which could lead to an increased level of eccentricity. However, this force does not directly affect the torque, and thus, it is not considered in the following.

Tests are conducted with a mass $m = 77$ g at $r = 50$ mm, leading theoretically to an amplitude $\Gamma_c = 0.04$ N · m. In order to reduce centrifugal forces and vibration, the motor is supplied at frequency $f_s = 25$ Hz. The PSD of the measured load torque with and without load unbalance is displayed in Fig. 13(b). An increase at rotational frequency $f_r \approx 12.5$ Hz is clearly visible, demonstrating that a load unbalance leads to a measurable increase of torque oscillations at f_r.

The time-frequency analysis of the stator current yields the following results. The PWD of the stator current at small load is displayed in Fig. 14 for the healthy case and with the load unbalance. The oscillating interference structure is visible at $f_s \pm f_r/2 = 25 \pm 12.5$ Hz in the faulty case which corroborates the preceding considerations. The IF of these two signals is shown in Fig. 15(a). Oscillations exist in the healthy and faulty case. Therefore, the time waveform cannot indicate

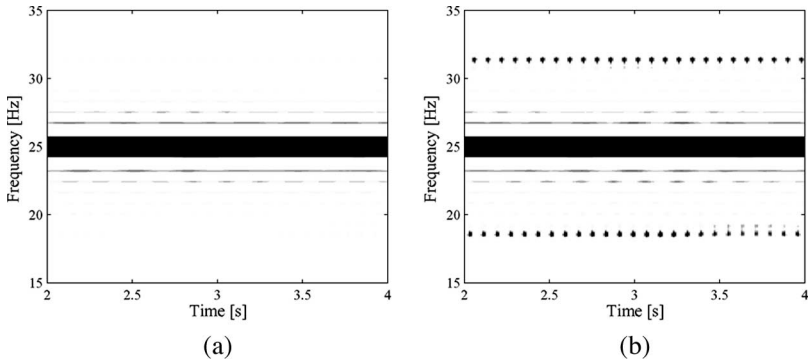

Fig. 14. PWD of stator current in healthy case and with unbalanced load, $f_s = 25$ Hz, small load. (a) Healthy. (b) Load unbalance.

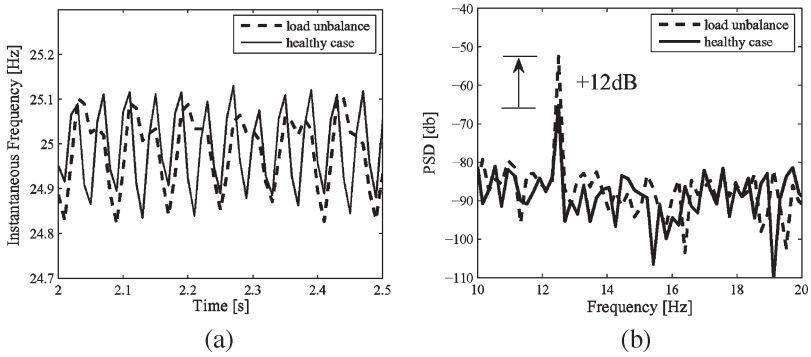

Fig. 15. IF and PSD of IF in healthy case and with unbalanced load, $f_s = 25$ Hz, small load. (a) IF. (b) PSD of IF.

the fault in this case due to the relatively small amplitude of Γ_c. However, the PSD of the IF [see Fig. 15(b)] shows an increase of more than 10 dB at f_r with the load unbalance. Therefore, it has been demonstrated that a more realistic fault such as a load unbalance can be detected using the proposed time-frequency stator current analysis.

VI. Conclusion

The present paper has examined the detection of mechanical fault-related load torque oscillations in induction motors using a stator current monitoring. An accurate theoretical analysis has shown the link between the torque oscillation and a phase modulation of a stator current component. Two classes of signal processing methods have been presented: classical spectral analysis and time-frequency analysis. The interest of time-frequency signal analysis in this context is the detection of the phase modulation, which is ambiguous using classical spectral analysis. Moreover, it is possible to detect the exact moment when the fault appears. The employed time-frequency methods are the WD and IF estimation. The theoretical considerations have been validated on simulation and experimental results. It has therefore been shown that time-frequency signal analysis represents a useful tool for current-based condition monitoring and mechanical fault detection.

Acknowledgment

The authors would like to thank O. Durrieu de Madron and R. Larroche for their help with the experimental setup.

References

[1] W. T. Thomson, "On-line current monitoring to detect electrical and mechanical faults in three-phase induction motor drives," in *Proc. Int. Conf. Life Manage. Power Plants*, Dec. 1994, pp. 66–73.
[2] R. R. Schoen and T. G. Habetler, "Effects of time-varying loads on rotor fault detection in induction machines," *IEEE Trans. Ind. Appl.*, vol. 31, no. 4, pp. 900–906, Jul./Aug. 1995.
[3] R. R. Obaid, T. G. Habetler, and D. J. Gritter, "A simplified technique for detecting mechanical faults using stator current in small induction motors," in *Proc. IEEE Ind. Appl. Soc. Annu. Meeting*, Rome, Italy, Oct. 2000, pp. 479–483.
[4] S. J. Yang, *Low-Noise Electrical Motors*. Oxford, U.K.: Clarendon, 1981.
[5] P. L. Timár, *Noise and Vibration of Electrical Machines*. North-Holland: Elsevier, 1989.
[6] J. R. Cameron and W. T. Thomson, "Vibration and current monitoring for detecting airgap eccentricities in large induction motors," *Proc. Inst. Electr. Eng.*, vol. 133, no. 3, pp. 155–163, May 1986.
[7] D. G. Dorrell, W. T. Thomson, and S. Roach, "Analysis of airgap flux, current, and vibration signals as a function of the combination of static and dynamic airgap eccentricity in 3-phase induction motors," *IEEE Trans. Ind. Appl.*, vol. 33, no. 1, pp. 24–34, Jan./Feb. 1997.
[8] M. Blödt, P. Granjon, B. Raison, and G. Rostaing, "Models for bearing damage detection in induction motors using stator current monitoring," in *Proc. IEEE ISIE*, Ajaccio, France, May 2004, pp. 383–388.
[9] B. Boashash, *Time Frequency Signal Analysis and Processing—A Comprehensive Reference*, 1st ed. Oxford, U.K.: Elsevier, 2003.
[10] P. Flandrin, *Time-Frequency/Time-Scale Analysis*. San Diego, CA: Academic, 1999.
[11] S. M. Kay, *Modern Spectral Estimation: Theory and Application*. Englewood Cliffs, NJ: Prentice-Hall, 1988.
[12] L. W. Couch, *Digital and Analog Communication Systems*, 4th ed. Englewood Cliffs, NJ: Prentice-Hall, 1993.
[13] W. Mecklenbräuker and F. Hlawatsch, Eds., *The Wigner Distribution—Theory and Applications in Signal Processing*, Amsterdam, The Netherlands: Elsevier, 1997.
[14] C. D. Cantrell, *Modern Mathematical Methods for Physicists and Engineers*. Cambridge, U.K.: Cambridge Univ. Press, 2000.

[15] V. Devanneaux, H. Kabbaj, B. Dagues, and J. Faucher, "A versatile model of squirrel cage induction machines for design, monitoring and diagnosis purposes," in *Proc. 9th EPE*, Graz, Austria, Aug. 2001.
[16] F. Auger, P. Flandrin, P. Gonçalvès, and O. Lemoine. (1995/1996). *Time-Frequency Toolbox*, France: CNRS/Rice Univ. [Online]. Available: http://tftb.nongnu.org

Martin Blödt (S'04) was born in Baden-Baden, Germany, in 1978. He received the double diploma degree in electrical engineering from the University of Karlsruhe (TH), Karlsruhe, Germany and from the Institut National Polytechnique de Grenoble (INPG), France, in 2003. He is currently working toward the Ph.D. degree at Laboratoire d'Electrotechnique et d'Electronique Industrielle (LEEI).

In 2003, he joined LEEI. His research interests include fault diagnosis in electrical machines and suitable signal processing methods such as time-frequency signal processing and parameter estimation.

Marie Chabert was born in 1970. She received the engineering degree from ENSEEIHT, Toulouse, France, in 1994, and the Ph.D. degree from the Institut National Polytechnique de Toulouse, Toulouse, in 1997.

In 1998, she joined ENSEEIHT and TéSA-IRIT as an Assistant Professor, where she teaches signal and image processing and telecommunications at the undergraduate and graduate level. Her research interests include estimation, detection, and wavelet transform. She has coauthored about 30 communications and papers in signal processing conferences and journals.

Jérémi Regnier received the Ph.D. degree in electrical engineering from the Institut National Polytechnique de Toulouse, Toulouse, France, in 2003.

Since 2004, he has been working as an Assistant Professor with the Electrical Engineering and Control Systems Department. He is also a Researcher with the Laboratoire d'Electrotechnique et d'Electronique Industrielle (LEEI), Toulouse. His research interests include modeling and simulation of faulty electrical machines and drives as well as the development of monitoring techniques using signal processing methods.

Jean Faucher (M'06) received the diploma degree in electrical engineering from the Institut National Polytechnique (INP) de Toulouse, Toulouse, France, in 1967, and the Docteur-Ingénieur (Ph.D.) and Docteur ès Sciences degrees on switched reluctance machines, in 1969 and 1981, respectively.

Since 1985, he has been a Full University Professor with INP Toulouse, teaching in electrical and control engineering. He is a Researcher with the Laboratoire d'Electrotechnique et d'Electronique Industrielle, Toulouse. His research interests include information processing and modeling of electrical machines and static converters for fault diagnosis, monitoring, and simulation. He is in charge of international relationships for INP Toulouse.